1 April 2000

ELSEVIER

Optics Communications 176 (2000) 339–345

OPTICS COMMUNICATIONS

www.elsevier.com/locate/optcom

Laboratory and field demonstration of a low cost membrane mirror adaptive optics system

David Dayton [a,*], Sergio Restaino [b], John Gonglewski [b], Joe Gallegos [c], Scot McDermott [d], Steve Browne [e,1], Sam Rogers [f,2], Mohan Vaidyanathan [g], Mike Shilko [g]

[a] *Applied Technology Associates, 1900 Randolph SE, Albuquerque, NM 87106, USA*
[b] *Air Force Research Laboratory, Directed Energy Directorate, Kirtland AFB, NM 87117, USA*
[c] *Boeing North America, Kirtland AFB, NM 87117, USA*
[d] *Logicon Advanced Technology, 2600 Yale SE, Albuquerque, NM 87106, USA*
[e] *The Optical Sciences, 1341 S. Sunkist Ave., Anaheim, CA 92806, USA*
[f] *Willow Systems, PO Box 11849, Albuquerque, NM 87192, USA*
[g] *ITT Advanced Engineering Div., 6400 Uptown Blvd., Albuquerque, NM 87110, USA*

Received 3 December 1999; accepted 5 January 2000

Abstract

We present here results of laboratory and field experiments using the OKO technologies membrane mirror as an adaptive optics device. The device can be operated at high temporal bandwidths from a low cost PC based control system. We have constructed a complete adaptive optics system costing less than twenty thousand dollars. In this paper we present results from this system used both in laboratory tests and on a one meter telescope located at Apache Point, New Mexico. © 2000 Elsevier Science B.V. All rights reserved.

PACS: 95.75.Qr; 07.10.Cm
Keywords: Adaptive optics; Micro-machined membrane mirror

1. Introduction

Micro-machined membrane mirrors have recently been developed as a compact low cost adaptive optic. Typical devices consist of a silicon chip mounted over a printed circuit board holder. The chip contains a silicon nitride membrane, which is coated with aluminum to form a mirror. An array of electrodes is etched onto the printed circuit board under the membrane. When an electrode is energized, an electrostatic force is produced on the portion of the membrane above the electrode, causing the mirror surface to deform. A schematic of such a device is shown in Fig. 1.

The electrode pattern for the OKO Technologies 37 actuator device [1] is shown in Fig. 2. The electrodes are arranged in a hexagonal pattern. The

* Corresponding author. Tel.: +1-505-853-6598; fax: +1-505-846-6132; e-mail: dayton@mail.aptec.com
[1] E-mail: sbrowne@tosc.com
[2] E-mail: srogers@willowsystems.com

0030-4018/00/$ - see front matter
PII: S0030-4018(00)00487-9

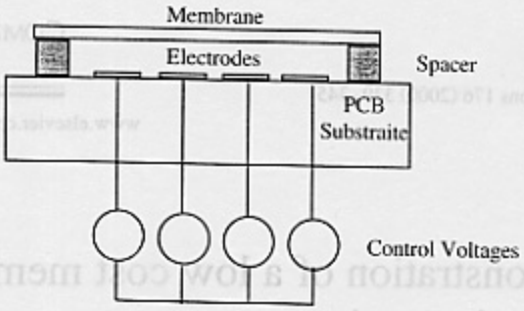

Fig. 1. Schematic of membrane mirror.

diameter of the membrane is 15 mm, with the membrane fixed to the edges of the circular aperture. The center to center spacing of the electrodes is 1.75 mm. This gives the center to center separation of the two end electrodes, along a radial, as 10.5 mm, or 70% of the full 15 mm aperture. Since the membrane is fixed along the edges of its circular aperture, it cannot be controlled to an arbitrary shape near the edge. Thus we only control its shape over the central 70% of the membrane which lies above the electrode array.

2. Laboratory setup

In previous papers [2,3] we described analysis of the OKO mirror and open and closed loop control for disturbance generation, and aberration correction. The equation for a stretched membrane over a circular aperture with fixed edges, was solved. From this solution we were able to generate theoretical influence functions. Using the influence functions, we were able to generate fits to Zernike polynomials. In this report we describe a closed loop demonstration system built around the OKO mirror. The closed loop response was tested against static and dynamic aberrations, and a 3 dB closed loop bandwidth was measured. The entire system including mirror, computer, electronics and optics cost less than twenty thousand dollars. This can be compared to many presently used systems that cost several hundred thousand to a million dollars.

Fig. 2 shows the arrangement of the Shack–Hartmann lenslets, used in our wave front sensor, with respect to the membrane mirror electrodes. A square array Shack–Hartmann wave front sensor was used

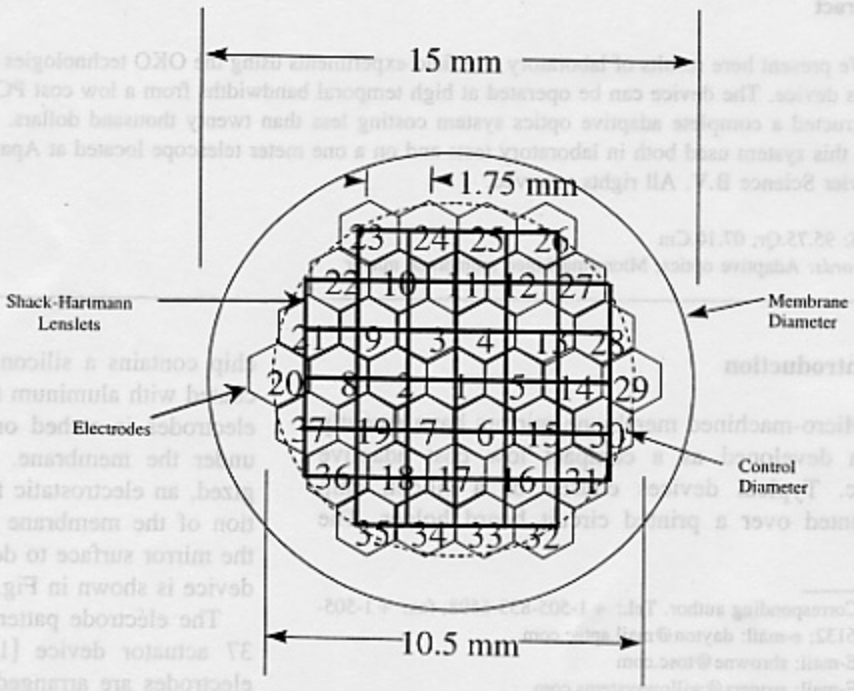

Fig. 2. Electrode pattern of the OKO membrane mirror with Shack–Hartmann lenslets overlaid.

rather than a hexagonal because the square geometry matched that of the pupil plane detector array. The Shack–Hartmann lenslet array that was used consisted of an array of 600 μm diameter lenslets in a square array, with 72 mm focal lengths.

Fig. 3 shows a diagram of the laboratory setup used to test the algorithm properties for controlling the OKO mirror. A phase shifting front end is attached to the Zygo interferometer. The Zygo beam provides a collimated source to the membrane mirror. The beam reflected from the membrane mirror passes through a beam splitter cube. Half the light is reflected to a focusing lens and a far field camera. This arrangement allows us both to look at the surface deformation of the mirror and the far field spot produced by this deformation. This was useful for troubleshooting the control loop.

The wave front sensor camera was a Dalsa CA-D1-0128A 128×128 pixel 8 bit camera capable of running up to 750 frames per second. We ran it with an exposure time of 1.3 ms. The focal plane camera used to record open and closed loop focal plane data was a 256×256 12 bit Dalsa camera model CA-2048M-014J. It was run with 10 ms exposures. Imaging Technology frame grabbers were used with both cameras. Two twenty channel D/A converters were used to drive the high voltage amplifiers that control the electrostatic actuators of the mirror. A fast photographic enlarger lens was used to re-image the Shack–Hartmann spots onto the wave front sensor detector array.

Note that the membrane mirror is mounted on a tip–tilt drive stage. Since the mirror is small and light weight it can be mounted directly to the stage. This allows off-loading of tip and tilt control from the mirror without a separated tip–tilt control loop.

3. Controlling the membrane mirror

The membrane mirror influence functions can be calculated by solving the second order equation for the surface of a stretched membrane with fixed circular boundary conditions.

$$\nabla^2 S(\rho,\phi) = -\frac{\varepsilon V(\rho,\phi)^2}{Td^2} \tag{1}$$

where S is the surface deformation, V is applied voltage, T is membrane tension, and d is the separation between the membrane and the electrodes. Ref. [4] gives a detailed approach for solving Eq. (1) to calculate influence functions for each of the mirror actuators.

The calculated influence functions over one quadrant of the mirror are shown in Fig. 4. Since the

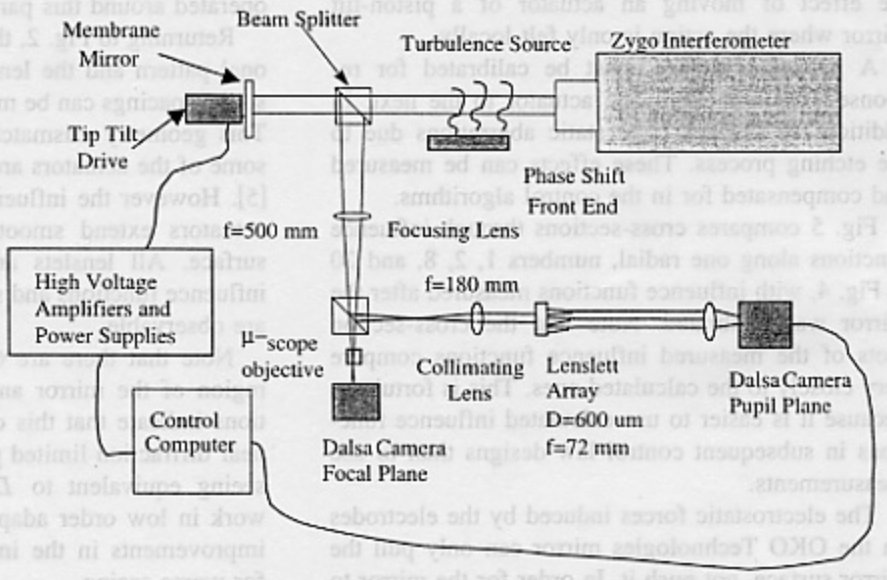

Fig. 3. Laboratory setup of the membrane mirror control system.

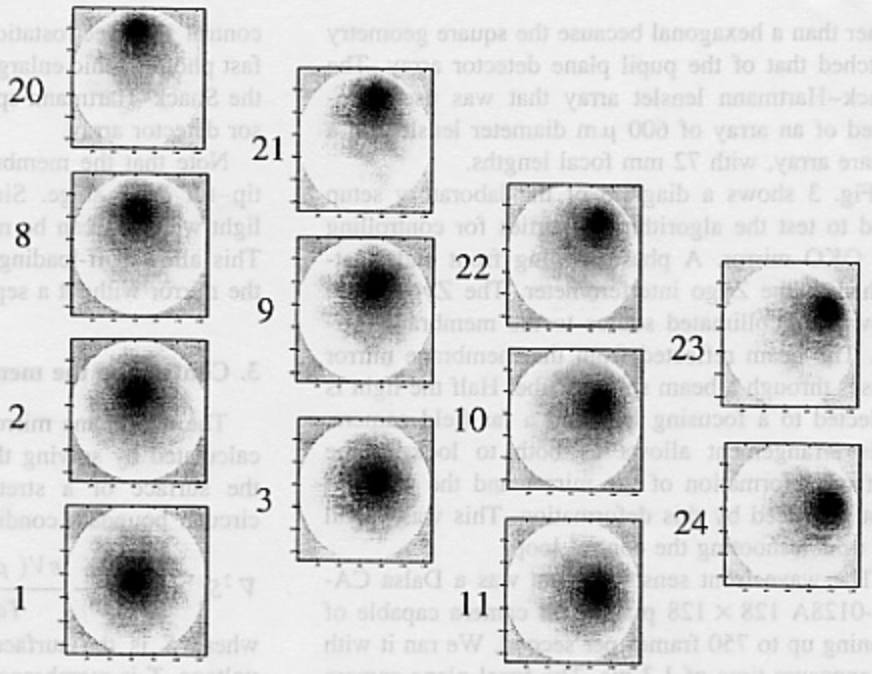

Fig. 4. Calculated influence functions of the membrane mirror electrodes.

mirror is circularly symmetric, the influence functions in the other three quadrants will be the mirror images of the ones shown. The effect of energizing one electrode is felt globally. This is in contrast to the effect of moving an actuator of a piston-tilt mirror where the action is only felt locally.

A particular device must be calibrated for response variations from one actuator to the next. In addition the devices have static aberrations due to the etching process. These effects can be measured and compensated for in the control algorithms.

Fig. 5 compares cross-sections through influence functions along one radial, numbers 1, 2, 8, and 20 in Fig. 4, with influence functions measured after the mirror was calibrated. Note that the cross-section plots of the measured influence functions compare very closely to the calculated ones. This is fortuitous because it is easier to use calculated influence functions in subsequent control law designs than to use measurements.

The electrostatic forces induced by the electrodes on the OKO Technologies mirror can only pull the mirror surface, not push it. In order for the mirror to operate with positive and negative deflections, the electrodes must be biased to half their maximum throw. When this is done, the mirror surface will assume a parabolic shape and the mirror can be operated around this parabolic bias.

Returning to Fig. 2, the electrodes are on a hexagonal pattern and the lenslets are in a square pattern so the spacings can be matched in only one direction. This geometry mismatch means that the actions of some of the actuators are observed better than others [5]. However the influence functions of each of the actuators extend smoothly over the entire mirror surface. All lenslets are effected by each of the influence functions and so the actions of all actuators are observable.

Note that there are 6 lenslets across the control region of the mirror and seven electrodes. Simulations indicate that this configuration should provide near diffraction limited performance for atmospheric seeing equivalent to $D/r0 = 6$ or less. However work in low order adaptive optics [6] indicates that improvements in the images should be noted even for worse seeing.

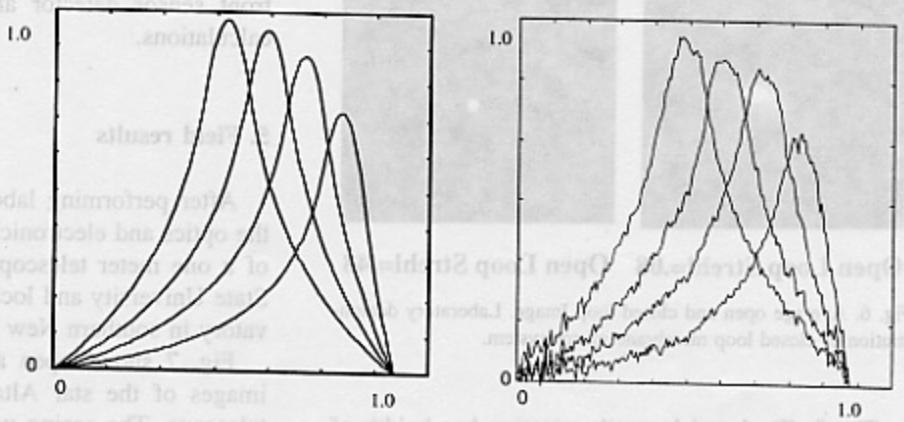

Calculated **Measured**

Fig. 5. Cross-sections through the center of the radial modes.

The Shack–Hartmann wave front sensor produces estimates of horizontal and vertical phase gradients across the center of the lenslet apertures by measuring the displacement of the centroid of the spot produced by each lenslet. A multi-input multi-output (MIMO) control matrix can be developed by fitting the influence functions to the phase gradient measurements.

The phase gradients can be expressed in matrix form as a function of the wave front phase.

$$\begin{bmatrix} \nabla_x \\ \cdots \\ \nabla_y \end{bmatrix} = \Gamma\Phi. \tag{2}$$

We assume that the wave front introduced by the mirror is a linear superposition of the mirror modes times the force exerted by an electrode

$$\Phi = \frac{a^2}{T}\sum_i A_i F_i \tag{3}$$

or in matrix form

$$\Phi = \frac{a^2}{T} AF \tag{4}$$

where A represents the mirror modes and F represents the vector of forces applied to the electrodes. Substituting Eq. (4) into Eq. (2) we get

$$\begin{bmatrix} \nabla_x \\ \cdots \\ \nabla_y \end{bmatrix} = \frac{a^2}{T}\Gamma AF. \tag{5}$$

A least squares fit to an arbitrary set of phase gradient measurements can be obtained by performing a least squares inverse of the matrix ΓA. This is shown in Eq. (6).

$$F = \frac{T}{a^2}[\Gamma A]^T\left[(\Gamma A)^T(\Gamma A)\right]^{-1}\begin{bmatrix} \nabla_x \\ \cdots \\ \nabla_y \end{bmatrix}. \tag{6}$$

Eq. (6) shows a matrix relationship that produces a vector of actuator electrode commands from a vector of gradient measurements. This vector is then applied to an integral controller with a user specified gain which drives the membrane mirror. The term T/a^2 can we absorbed into the gain and so does not need to be known explicitly.

The integrator gain was set in the following manner. The gain was increased until the control loop just started to become unstable. Then the gain was reduced by 10% and the control loop operated at this point.

4. Laboratory results

A laboratory demonstration of the closed loop adaptive optics system was performed using a soldering iron and fan as a turbulence source. In this way we were able to introduce a turbulence strength of $D/r0 \sim 6$, with a Greenwood frequency of 20 or 30 Hz. Fig. 6 shows the average of 100 frames of data, both open and closed loop.

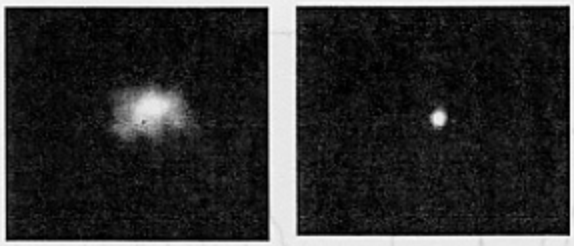

Open Loop Strehl=.08 **Open Loop Strehl=.48**

Fig. 6. Average open and closed loop Image. Laboratory demonstration of closed loop membrane mirror system.

The 3 dB closed loop tilt rejection bandwidth of the membrane mirror control system was measured at 50 Hz. This was done by driving the tip–tilt stage, on which the mirror was mounted, at different sinusoidal frequencies. We then closed the membrane control loop and measured the tip–tilt rejection as a function of frequency. The bandwidth is primarily limited by the time required to read out the wave front sensor detector array and make the control calculations.

5. Field results

After performing laboratory tests we repackaged the optics and electronics to fit at the Nysmith focus of a one meter telescope operated by New Mexico State University and located at Apache Point Observatory in southern New Mexico.

Fig. 7 shows open and closed loop focal plane images of the star Altair taken on the one meter telescope. The seeing was between 8 and 10 cm or $D/r0 = 10$–12. Note that the closed loop images include a diffraction limited core surrounded by a diffuse speckle halo. This is due the fact that the membrane mirror in conjunction with the wave front sensor cannot fully correct for this level of turbulence. None the less we still see an improvement in the closed loop Strehl ratio from about 0.04 to 0.1.

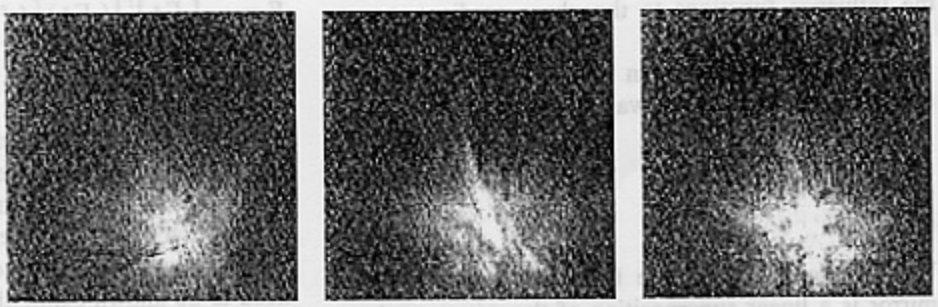

Open Loop Strehl Ratio = .04

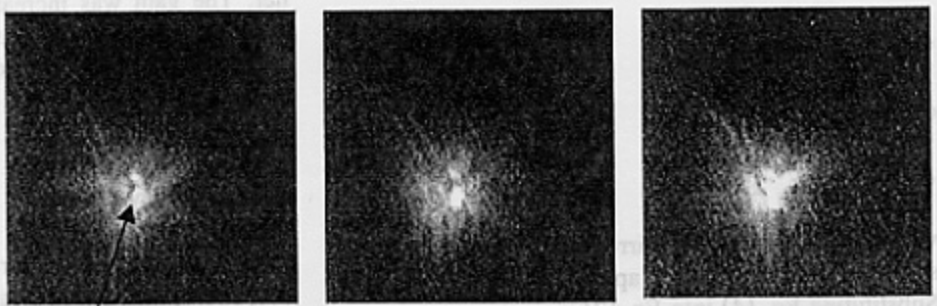

Closed Loop Strehl Ratio = .1

Fig. 7. Open and closed loop images of Altair on a one meter telescope at Apache Point, New Mexico, 10 ms exposures.

6. Conclusions

In summary we have developed a low cost adaptive optic system based around the OKO technologies membrane mirror. Laboratory tests indicate that the system can provide full order correction of a turbulence disturbance equivalent to $D/r0 = 6$ with a closed loop 3 dB bandwidth of 50 Hz. Experiments on a one meter telescope indicate that the system can provide improvements in images for disturbances as strong as $D/r0 = 10$. The entire system as mounted and operated on the one meter telescope cost less than twenty thousand dollars.

We have examined the equations that govern the surface shape of an ideal membrane mirror. The geometry of the OKO technologies membrane mirror was analyzed. Ideal influence functions were calculated and compared to measured influence function with close agreement. The calculated influence functions were then used to develop a closed loop multi-input multi-output control law for the device.

References

[1] G. Vdovin, Opt. Commun. 115 (1995) .
[2] D. Dayton, J. Gonglewski, SPIE 3760 (1999) .
[3] D. Dayton, J. Gonglewski, SPIE 3866 (1999) .
[4] E. Claflin, N. Bareket, J. Opt. Soc. Am. A 3 (1986) 11.
[5] M. Furber, D. Jordan, Opt. Eng. 36 (1997) 7.
[6] M. Roggeman, Appl. Opt. 30 (1991) 29.